Journal of proteome research

Article

pubs.acs.org/jpr

Compensatory Islet Response to Insulin Resistance Revealed by Quantitative Proteomics

Abdelfattah El Ouaamari,[†,∥] Jian-Ying Zhou,[‡,∥] Chong Wee Liew,[§,∥] Jun Shirakawa,[†,⊥] Ercument Dirice,[†,⊥] Nicholas Gedeon,[†] Sevim Kahraman,[†] Dario F. De Jesus,[†] Shweta Bhatt,[†] Jong-Seo Kim,[‡] Therese R. W. Clauss,[‡] David G. Camp, II,[‡] Richard D. Smith,[‡] Wei-Jun Qian,[*,‡] and Rohit N. Kulkarni[*,†]

[†]Islet Cell & Regenerative Biology, Joslin Diabetes Center, Department of Medicine, Brigham and Women's Hospital, Harvard Medical School, Boston, Massachusetts 02215, United States

[‡]Biological Sciences Division and Environmental Molecular Sciences Laboratory, Pacific Northwest National Laboratory, Richland, Washington 99352, United States

[§]Department of Physiology and Biophysics, University of Illinois at Chicago, Chicago, Illinois 60612, United States

Supporting Information

ABSTRACT: Compensatory islet response is a distinct feature of the prediabetic insulin-resistant state in humans and rodents. To identify alterations in the islet proteome that characterize the adaptive response, we analyzed islets from 5 month old male control, high-fat diet fed (HFD), or obese ob/ob mice by LC−MS/MS and quantified ∼1100 islet proteins (at least two peptides) with a false discovery rate < 1%. Significant alterations in abundance were observed for ∼350 proteins among groups. The majority of alterations were common to both models, and the changes of a subset of ∼40 proteins and 12 proteins were verified by targeted quantification using selected reaction monitoring and western blots, respectively. The insulin-resistant islets in both groups exhibited reduced expression of proteins controlling energy metabolism, oxidative phosphorylation, hormone processing, and secretory pathways. Conversely, an increased expression of molecules involved in protein synthesis and folding suggested effects in endoplasmic reticulum stress response, cell survival, and proliferation in both insulin-resistant models. In summary, we report a unique comparison of the islet proteome that is focused on the compensatory response in two insulin-resistant rodent models that are not overtly diabetic. These data provide a valuable resource of candidate proteins to the scientific community to undertake further studies aimed at enhancing β-cell mass in patients with diabetes. The data are available via the MassIVE repository, under accession no. MSV000079093.

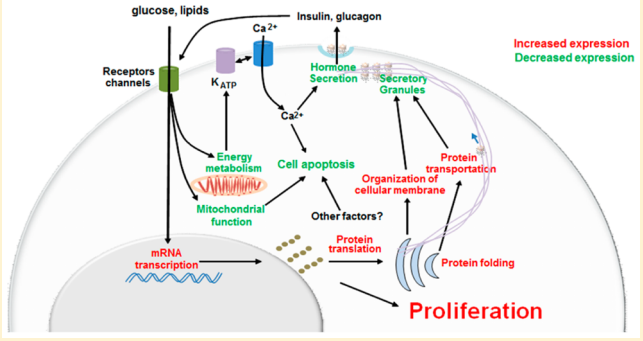

KEYWORDS: *Insulin resistance, pancreatic islets, proteome, proliferation, metabolism, function*

INTRODUCTION

Type 2 diabetes has reached epidemic proportions worldwide and impacts multiple organ systems. Following the development of insulin resistance, the onset of the disease is triggered when the residual functional β-cells fail to compensate for the increased metabolic needs of the individual.[1] Despite available insulin-based and oral hypoglycemic medications, the disease continues to spread worldwide and is predicted to affect over 360 million individuals globally by 2030.[2] Genome-wide association studies revealed that type 2 diabetes-linked genes are involved in regulating β-cell mass as well as function,[3] suggesting the relevance of targeting β-cells as a therapeutic strategy for type 2 diabetes. Although islet transplantation has achieved success in reversing the disease and limiting its complications,[4] the shortage of islets from donors has prompted a reconsideration of designing alternative therapies.

While it is still debatable whether therapies should target enhancing insulin secretion from residual β-cells or increasing the number of functional insulin-producing cells,[5] insights to design efficient therapeutics might emerge from an understanding of the processes by which β-cells compensate for a chronic increased demand for insulin. Indeed, obese nondiabetic individuals develop a compensatory islet β-cell response to adjust the levels of insulin to counteract insulin resistance and therefore maintain normoglycemia. Generally speaking, humans with insulin resistance (e.g., impaired fasting glucose or pregnancy) exhibit increased insulin secretion as compared to that in controls.[6] However, whether this compensatory response is attributed to structural or functional

Received: January 21, 2015
Published: July 7, 2015

DOI: 10.1021/acs.jproteome.5b00587
J. Proteome Res. 2015, 14, 3111−3122

adaptation of islet β-cells is incompletely understood. Although increased β-cell proliferation in metabolically challenged rodents is known as a major structural adaptive response within islets,[7] the proportional contribution of functional changes in islet cells is unclear. Most studies that have investigated islet cell function in the context of insulin resistance were performed *in vivo*,[1a] where the islet cell mass is a considerable confounder, and fewer *in vitro* metabolic studies have been undertaken in rat islets.[8] Several proteomics studies were performed on islets derived from insulin-resistant diabetic mice.[9] However, these studies did not address adaptive functional molecular changes in islet cells in response to insulin resistance but rather dysfunction of islet β-cells in diabetes. In one study, the diabetic MKR (a transgenic mouse with a dominant-negative IGF-1R in skeletal muscle) mouse was used to investigate deleterious effects of insulin resistance on β-cell function.[9c] The same group reported a combined proteomic and microarray screen to assess defects occurring in insulin-resistance-induced β-cell failure.[9b] Interestingly, a proteomics screen was used to address the transition from obesity to diabetes in the Zucker fatty (ZF) and Zucker diabetic fatty (ZDF) rat models.[9a] Finally, a two-dimensional gel electrophoresis approach was applied to identify proteomic changes in the entire pancreas derived from db/db or C57BL/6J mice challenged with high-fat diet (HFD); however, a major limitation in these studies was a lack of distinction between acinar and islet cells.[9d,10]

Herein, we used a comparative proteomics approach to characterize changes in the islet proteome in two commonly used insulin-resistant prediabetic models, ob/ob (small or large islets) and HFD mice. Ingenuity Pathway Analysis of the significantly altered proteins revealed an intriguing down-regulation of major proteins involved in pathways critical for hormone secretion, including glucose and amino acid metabolism, Krebs cycle, mitochondrial oxidative phosphorylation, hormone biosynthesis, and the final steps of exocytosis, suggesting functional maladaptation of islet cells in insulin-resistance states. Moreover, increased protein synthesis and vesicular transport were observed, indicating endoplasmic reticulum (ER) stress in insulin-resistant islets. Interestingly, several proteins known to control cell proliferation and survival were upregulated in both HFD and ob/ob islets as compared to controls. Finally, it is notable that most proteomic changes were observed in both models of insulin resistance as well as in both small and large islets. These data provide a comprehensive view of proteomic changes occurring during obesity-induced islet hyperplasia and provide potential opportunities for therapeutic strategies to address β-cell decline in diabetic states.

EXPERIMENTAL PROCEDURES

Islet Isolation

Islets from 5 month old C57BL/6 male high-fat diet (HFD) fed and obese ob/ob mice ($n = 6$) manifesting insulin resistance as well as from age-matched control C57BL/6 male mice were isolated by the intraductal enzyme injection technique using liberase.[11] Briefly, the pancreas was inflated with liberase, and islets were isolated as reported previously.[12] All islets were cultured overnight at physiological glucose levels (7 mM glucose, 10% FBS) to allow the islets to recover from the effects of liberase digestion. Islets were then transferred to nuclease- and pyrogen-free tubes and washed with phosphate buffer. Following removal of the buffer, pellets were frozen at −80 °C prior to proteomic analyses.

Protein Digestion

Islet samples were homogenized and digested using a 2,2,2-trifluoroethanol (TFE)-based protocol.[13] Briefly, islets were dissolved in 30 μL of 50% TFE/50% 25 mM NH_4HCO_3 by 3 min sonication in a 5510 Branson ultrasonic water bath (Branson Ultrasonics, Danbury, CT) with ice-cold water. Protein concentration was determined by BCA assay. About 40 μg of islet proteins from each mouse was denatured in 50% TFE for 105 min at 60 °C, reduced by 2 mM DTT for 60 min at 37 °C, diluted 5-fold with 50 mM NH_4HCO_3, and digested by 0.8 μg of trypsin (1:50 w/w trypsin-to-protein ratio) for 3 h at 37 °C. The digestion was stopped by 0.1% TFA. All peptide samples were dried in a SpeedVac remove TFE , and resuspended in 25 mM NH_4HCO_3 for LC−MS/MS analysis.

LC−MS/MS Analysis

LC−MS/MS analyses were performed on a custom-built automated LC system coupled online to an LTQ-Orbitrap mass spectrometer (Thermo Scientific, San Jose, CA) via a nanoelectrospray ionization interface as previously described.[14] Briefly, 0.75 μg of peptides was loaded onto a homemade 65 cm long reversed-phase capillary column with 75 μm i.d. packed using 3 μm Jupiter C18 particles (Phenomenex, Torrance, CA). The mobile phase was held at 100% A (0.1% formic acid) for 20 min, followed by a linear gradient from 0 to 60% buffer B (0.1% formic acid in 90% acetonitrile) over 85 min. The instrument was operated in data-dependent mode with an m/z range of 400−2000, in which a full MS scan with a resolution of 100 K was followed by six MS/MS scans. The six most intensive precursor ions were dynamically selected in the order of highest to lowest intensity and subjected to collision-induced dissociation using a normalized collision energy setting of 35% and a dynamic exclusion duration of 1 min. The heated capillary was maintained at 200 °C, and the ESI voltage was kept at 2.2 kV.

MS/MS Data Analysis

LC−MS/MS raw data were converted into .dta files using Extract_MSn (version 3.0) in Bioworks Cluster 3.2 (Thermo Fisher Scientific, Cambridge, MA), and the SEQUEST algorithm (version 27, revision 12) was used to search all MS/MS spectra against a mouse protein FASTA file that contains 16 244 entries (UniProt, released on April 20, 2010). The search parameters used were as follows: dynamic oxidation of methionine, 3 Da tolerances for precursor ion masses, and 1 Da for fragment ion masses. The search parameter file did not include any enzyme cleavage restraints on the termini of the identified peptides, which means that both tryptic peptides and nontryptic peptides were identified during database searching and that tryptic rules were applied only during data filtering steps. Moreover, the search parameter file allowed a maximum of three trypsin miscleavage sites for any given peptide identification. MS generating-function (MSGF) scores were generated for each identified spectrum as described previously by computing rigorous p-values (spectral probabilities).[15] Fully tryptic peptides with a MSGF score $< 5 \times 10^{-10}$ and mass measurement errors < 3 ppm were accepted as identifications. All peptides that passed the filtering criteria were input into the ProteinProphet program[16] to generate a final nonredundant list of proteins. The decoy-database searching methodology[13,17] was used to control the FDR at the unique peptide level to

DOI: 10.1021/acs.jproteome.5b00587
J. Proteome Res. 2015, 14, 3111−3122

<0.5%. The LC−MS/MS raw data along with Sequest output files have been deposited into the MassIVE repository, under accession no. MSV000079093. The data was also shared with ProteomeXchange and assigned data set identifier PXD002009.

Label-Free Quantification

Label-free MS intensity-based quantification was performed using the accurate mass and time (AMT) tag approach as previously described.[18] Briefly, the islet AMT tag database was populated based on all the confident peptide identifications from the MS/MS data, and the theoretical masses and observed normalized elution time (NET) values for each identified peptide were included in the database. The AMT tag database essentially serves as a look-up table for LC−MS feature identifications. LC−MS data sets were automatically analyzed using an in-house-developed software package that included Decon2LS and VIPER informatics software tools.[19] Initial analysis of the raw LC−MS data involved the use of Decon2LS to perform a deisotoping step, which generated a text file report for the detected masses and their corresponding intensities. Each data set was then processed by using the feature-matching tool VIPER to identify and quantify peptides. LC−MS feature identification was achieved by matching the accurately measured masses and NET values of each detected feature to the islet AMT tag database. Only when the measured mass and NET for each given feature matched the calculated mass and NET of a peptide in the AMT tag database within a 2 ppm mass error and 2% NET error were the features considered to be confidently identified as peptides.

The obtained abundance data (MS intensities) for all identified peptides from different data set were further processed by statistical data analysis software tool DAnTE.[20] The peptide abundance data were initially $\log_2$-transformed, normalized using the central tendency approach. Protein abundance profiles across different conditions were generated by taking a rescaling procedure for peptide profiles for each protein against a reference peptide.[18a] Statistical analysis using nested ANOVA was applied to identify proteins with significant abundance changes between different biological conditions by considering both biological replicates (n = 5) and technical replicates (n = 2). Proteins with significant abundance changes across the biological groups were identified by requiring a p-value < 0.01 and $\log_2$ ratio (over control) > 0.58 (corresponding to 50% change) in at least one of the conditions.

Preparation of ^{18}O-Labeled Peptide Reference Sample

The ^{18}O-labeled peptide reference sample was generated by trypsin-catalyzed ^{18}O labeling at the peptide level and was performed using a recently improved protocol.[21] Briefly, the reference sample pooled from all biological replicates was lyophilized to dryness and reconstituted in 100 μL of 50 mM NH_4HCO_3 in $H_2{}^{18}O$ (97%; ISOTEC, Miamisburg, OH), pH 7.8. One microliter of 1 M $CaCl_2$ and solution phase trypsin dissolved in $H_2{}^{18}O$ at a 1:50 trypsin/peptide ratio (w/w) were added to the samples. The tubes were wrapped in parafilm and mixed continuously for 5 h at 37 °C. The reaction was stopped by boiling the sample in a water bath for 10 min. After snap freezing the sample in liquid nitrogen, the samples were acidified by adding 5 μL of formic acid, and final peptide concentrations were measured using a BCA assay.

Targeted Quantification Using Selected Reaction Monitoring (SRM)

SRM-based targeted quantification using ^{18}O-based reference[22] was performed for 39 selected proteins. The peptides and SRM transitions were selected and screened as previously described[22] and are listed in Supporting Information Table S7. At least six transitions of each peptide were monitored in initial screening to ensure the confident identification and detection of the targeted peptides. The best two transitions (without interference) for each peptide were selected for final quantification. The predicted collision energies from Skyline were used for all peptides. Prior to LC−SRM analyses, the ^{18}O-labeled reference sample was spiked into each peptide sample at a 1:1 mixing ratio. All peptide samples were analyzed on a Waters nanoACQUITY UPLC system (Waters Corporation, Milford, MA) directly coupled online to a triple quadrupole mass spectrometer (TSQ Vantage; Thermo Fisher Scientific) using a 25 cm long, 75 μm i.d. fused silica capillary column. One microliter aliquots of each sample containing ∼0.5 μg/μL peptides were injected onto the analytical column with a 40 min linear gradient of 10−50% acetonitrile and 0.1% formic acid. A fixed dwell time of 10 ms and a scan window of 0.002 m/z were employed. All data sets were analyzed by Skyline software. The peak area ratios were used for the evaluation of protein abundance changes.

Western Blot and Antibodies

For western blotting, more than 150 isolated islets from 6 month old male C57BL/6 and age-matched male ob/ob mice were lysed in ice-cold M-PER buffer (Thermo Fisher Scientific) with protease inhibitor cocktail and phosphatase inhibitor cocktail (Sigma). After centrifugation, the extracts were subjected to western blotting with antibodies to CDK5Rap3 (Santa Cruz, no. sc-134627), Sel1l (Abcam, no. ab78298), Nucb2 (Abcam, no. ab30945), PCSK1 (Thermo Fisher, no. PA1-057), PCSK2 (Thermo Fisher, no. PA1-058), SYTL4 (Santa Cruz, no. sc-34446), UCN3 (Bioss, no. bs-2786R), VAMP2 (Thermo Fisher, no. PA1-766), COX7A2 (Life technologies, no. A21367), COX4I1 (Cell Signaling, no. 4850), MAOB (Abcam, ab125010), SDHB (Life technologies, no. A21345), or β-actin (Cell Signaling, no. 4697). Densitometry was performed using ImageJ software.

RESULTS

To examine islet proteome changes occurring during islet cell adaptation in the course of insulin resistance, we performed comprehensive LC−MS-based quantitative proteomic profiling using freshly isolated islets from 5 month old wild-type mice, age-matched leptin-deficient obese (ob/ob) mice, or mice challenged for 12 weeks with 60% kcal high-fat diet (HFD) beginning at 8 weeks of age. Moreover, to elucidate whether the insulin-resistance-induced islet compensatory response is distinct in populations of islets with variable size, we also compared the proteome of small (S, ∼50 μm) and large (L, ∼200 μm) islets from ob/ob mice, where the variability in islet size was greater compared to that in the HFD model. Mice in both models exhibited increased body weight, mild hyperglycemia (200 mg/dL), hyperinsulinemia in the fed state, and islet hyperplasia as compared to controls (Figure 1A−D).

LC−MS-based label-free quantification of samples isolated from control, ob/ob small, ob/ob large, or HFD islets (n = 5 for each group) resulted in confident identification and quantification of ∼6900 unique peptides and ∼1100 proteins

DOI: 10.1021/acs.jproteome.5b00587
J. Proteome Res. 2015, 14, 3111−3122

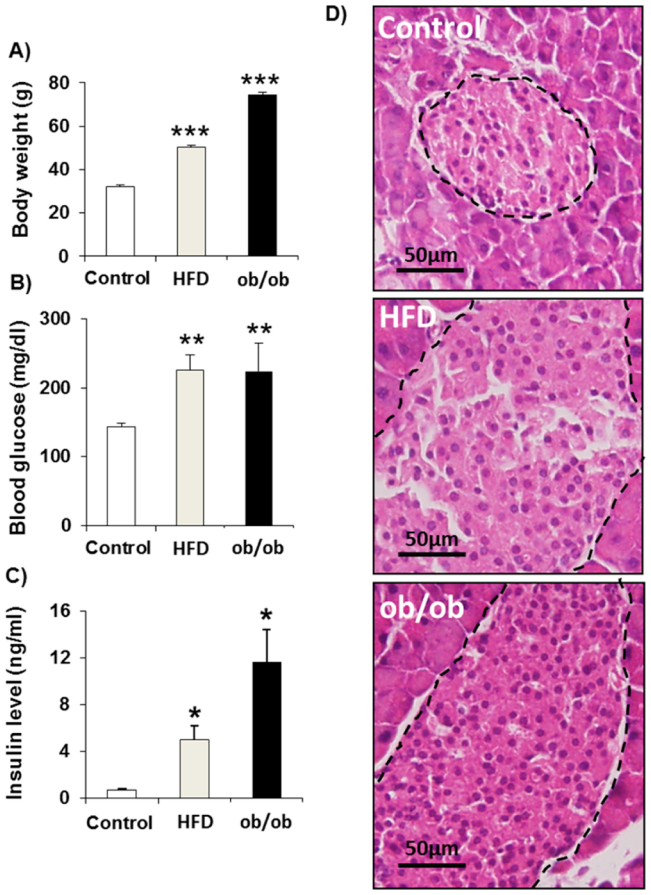

Figure 1. Characteristics of HFD and ob/ob mice. (A) Body weights. (B) Random fed blood glucose. (C) Random fed insulin levels. (D) Hematoxylin and Eosin staining of pancreatic sections. Data represent mean ± SEM; * $p < 0.05$ based on Student's t test (n = 5–6 per group). HFD, high-fat diet mice; ob/ob, leptin-deficient mice. The black dashed lines in (D) indicate the islet contour, which shows the larger size of islets in HFD and ob/ob mice compared to that in the control.

with at least two peptides per protein applying the accurate mass and time (AMT) tag approach[18b] (Supporting Information Tables S1 and S6). Figure 2A,B illustrates the data analysis process, where the raw peptide abundance profiles for a given protein obtained by the AMT tag approach was displayed in Figure 2A using the data analysis tool DAnTE.[20] In Figure 2B, a protein abundance profile was obtained for the protein (blank curve) after rescaling and rolling up to the protein level. The high reproducibility of the quantitative approach was illustrated in the comparison of two technical replicates (Figure 2C), whereas the comparison between control and ob/ob (small islets) conditions shows more biological variation (Figure 2D). After subjecting the data to statistical analysis, approximately ~350 proteins were revealed to be significantly altered in either ob/ob or HFD mouse islets (Figure 2E and Supporting Information Table S2). Among the ~350 proteins, the majority displayed a relative small changes ($\log_2$ ratio < 1) for any given biological condition (HFD, ob/ob small, or ob/ob large), and only ~100 proteins exhibited more than a 2-fold change (Supporting Information Figure S1). Since we did not observe a significant difference between small and large islets from ob/ob mice, only data from the small islets from ob/ob mice are presented here.

To further validate the global quantitative data, targeted quantification using selected reaction monitoring (SRM), a multiplexed quantitative technology providing similar quality as that with western blot or immunoassays,[23] was applied to validate a select list of 39 proteins from different functional categories (Supporting Information Table S3). Selected examples of extracted ion chromatograms (XICs) for targeted peptides from SRM measurements are shown in Supporting Information Figure S2. Figure 2F shows that SRM measured abundance ratios (HF or ob/ob divided by control) for the 39 proteins correlate well with the abundance ratio data obtained from AMT tag-based global profiling, supporting the overall high quality of the global quantitative profiling.

Among the altered proteins, most of the changes were common between HFD and ob/ob models (Figure 2E). The subcellular components, molecular functions, and canonical pathways of the altered proteins were analyzed by Ingenuity Pathway Analysis (IPA), as shown in Figure 3. The distribution of altered proteins in subcellular components indicated that the majority of protein alterations occurred in the cytoplasm, which consisted of nearly one-third of the total quantified proteins in the category (Figure 3A). The observation that enzymes are the most altered category in molecular function (Figure 3B) corroborates well with cytoplasm as the main component of protein alterations. The canonical pathway analysis (Figure 3C) clearly indicated downregulation in mitochondrial function and metabolism and upregulation in translational regulation and stress-related signaling. Selected regulated proteins implicated in different functional categories (Table 1) were further examined in detail.

Metabolic and Mitochondrial Dysfunction

IPA analysis of the altered proteins revealed significant changes in glycolysis, gluconeogenesis, and Krebs cycle pathways (Table 1). Although aldo-keto reductase family 1, member A1 (AKR1A1), lactate dehydrogenase A (LDHA), and phosphoglucomutase 2 (PGM2) were found to be upregulated in insulin-resistance-derived islets, proteins regulating glycolysis/gluconeogenesis were observed to be downregulated. The downregulated proteins including aldehyde dehydrogenase 3 family, member A2 (ALDH3A2), aldolase A (ALDOA), dihydrolipoamide S-acetyltransferase (DLAT), dihydrolipoamide dehydrogenase (DLD), enolase 2 (ENO2), and phosphofructokinase, liver (PFKL). Moreover, several enzymes regulating citrate cycle were affected. Proteins belonging to isocitrate dehydrogenase family (IDH1, IDH2, and IDH3A), pyruvate carboxylase (PC), phosphoenolpyruvate carboxykinase 2 (PCK2), and succinate dehydrogenase complex, subunit B (SDHB) were downregulated in islets derived from both HFD and ob/ob models. Downregulation in mitochondrial function was detected in islets derived from HFD and ob/ob animals since the expression levels of several components of ATP synthase machinery, including ATP5I, ATP6 V1D, ATP5J2, ATP6 V1A, ATP6 V1B2, ATP6 V1F, and ATP6 V1H, were lower compared to control animals (Table 1 and Supporting Information Table S2). Furthermore, members of cyclooxygenase family were also affected. Thus, expression of COX4I1, COX5A, COX6A1, and COX7A2, cytochrome C1 (CYC1), and components of ubiquinol-cytochrome c reductase complex (UQCRC1, UQCRC2, UQCRFS1, and UQCRQ) were decreased in hyperplastic islets (Table 1 and Supporting Information Table S2). Notably, we found SOD2, a major

DOI: 10.1021/acs.jproteome.5b00587
J. Proteome Res. 2015, 14, 3111–3122

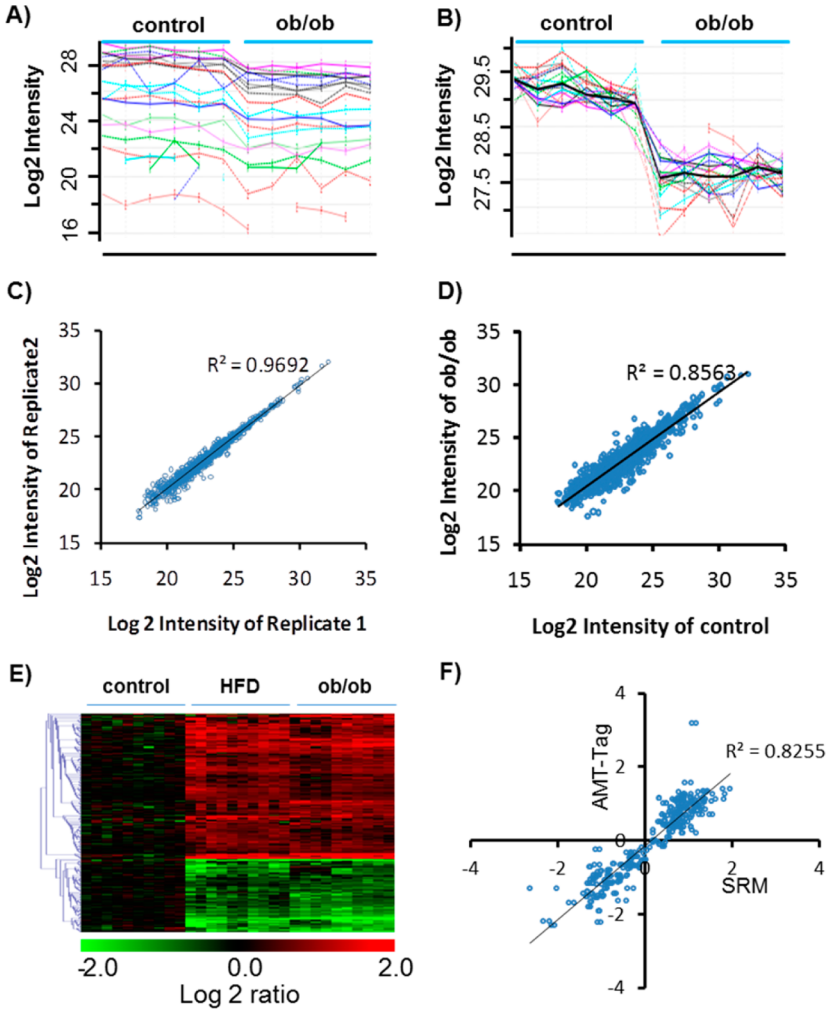

Figure 2. Quantitative analysis strategy for the islet proteome. (A) Raw peptide intensity profile data (log_2 transformed) of all peptides identified from glucagon. Each line profile represents a peptide from glucagon. Three control and three ob/ob (small islets) samples are presented, with each sample analyzed in duplicate. (B) Rescaled peptide intensity profile data. Dark line represents the protein abundance profile by averaging the intensity of all peptides after the rescaling process. (C) Reproducibility of protein abundance quantification between technical replicates. (D) Comparison of protein abundance between control and ob/ob (small islets). (E) Heatmap of all proteins with significant changes. Each condition has five biological replicates; each replicate has duplicate runs. Values are normalized to the average of the control. Only data from small islets from ob/ob mice are presented. (F) Validation of label-free quantitative data for selected proteins by selected reaction monitoring (SRM). Values are the log_2 ratios to control. Each data represents one protein under one condition summarized from five biological replicates. Data points from both HFD and ob/ob mice are included.

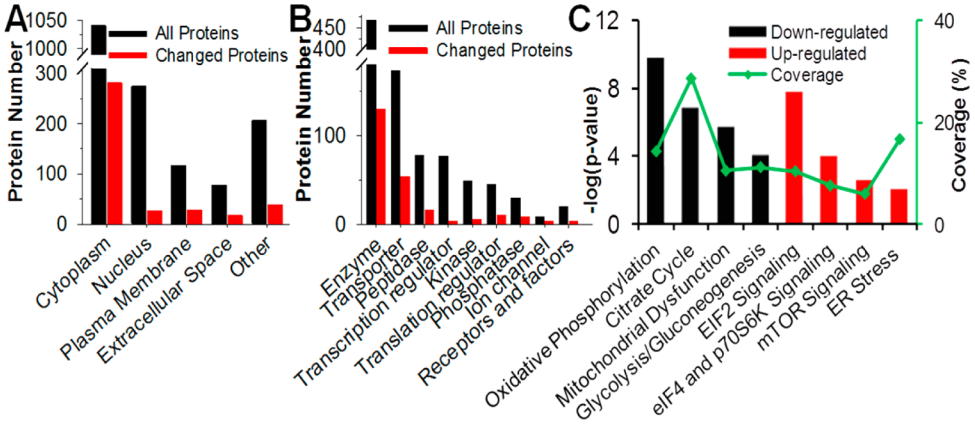

Figure 3. Functional analysis of quantified proteins. All quantified proteins were submitted to Ingenuity Pathway Analysis (IPA) to evaluate the biological function. Proteins were grouped based on subcellular location (A) or molecular functions (B). The major significantly downregulated (black) and upregulated (red) canonical pathways are presented in (C). Green line in (C) is the proteome coverage of each canonical pathway.

DOI: 10.1021/acs.jproteome.5b00587
J. Proteome Res. 2015, 14, 3111−3122

Table 1. List of Selected Altered Proteins Involved in Different Functional Categories[a]

gene symbol	protein name	$\log_2$ ratio ± SEM		
		HFD vs control	ob/ob (S) vs control	ob/ob (L) vs control
Glycolysis/Gluconeogenesis				
AKR1A1	Alcohol dehydrogenase [NADP+]	0.17 ± 0.08	0.47 ± 0.11	0.64 ± 0.04
LDHA	L-Lactate dehydrogenase A chain	0.12 ± 0.26	1.70 ± 0.15	2.10 ± 0.13
PGM2	Phosphoglucomutase-2	0.90 ± 0.06	0.77 ± 0.21	1.32 ± 0.05
ALDH3A2	Fatty aldehyde dehydrogenase	−0.03 ± 0.11	−0.28 ± 0.12	−0.6 ± 0.06
ALDOA	Fructose-bisphosphate aldolase A	−0.41 ± 0.07	−0.65 ± 0.08	−0.45 ± 0.03
ENO2	Gamma-enolase	−0.45 ± 0.10	−1.01 ± 0.10	−0.82 ± 0.16
PFKL	6-Phosphofructokinase, liver type	−0.65 ± 0.09	−0.72 ± 0.06	−0.73 ± 0.06
Citrate Cycle				
DLD	Dihydrolipoyl dehydrogenase	−0.39 ± 0.11	−0.78 ± 0.08	−0.70 ± 0.08
IDH1	Isocitrate dehydrogenase	−0.66 ± 0.10	−0.67 ± 0.13	−0.23 ± 0.13
IDH2	Isocitrate dehydrogenase	−0.81 ± 0.15	−1.25 ± 0.09	−1.20 ± 0.09
PC	Pyruvate carboxylase, mitochondrial	−0.8 ± 0.12	−1.10 ± 0.19	−1.42 ± 0.15
PCK2	Phosphoenolpyruvate carboxykinase	−0.65 ± 0.11	−0.52 ± 0.11	−0.87 ± 0.10
SDHB	Succinate dehydrogenase	−0.34 ± 0.08	−0.45 ± 0.05	−0.66 ± 0.08
Oxidative Phosphorylation and Mitochondrial Dysfunction				
ATP5I	ATP synthase subunit e, mitochondrial	−0.35 ± 0.12	−0.61 ± 0.13	−0.34 ± 0.02
ATP5J2	ATP synthase subunit f, mitochondrial	−0.02 ± 0.07	−0.13 ± 0.13	−0.60 ± 0.09
ATP6 V1A	V-type proton ATPase catalytic	−0.32 ± 0.09	−0.54 ± 0.05	−0.62 ± 0.03
COX5A	Cytochrome c oxidase subunit 5A	−0.34 ± 0.18	−0.59 ± 0.07	−0.58 ± 0.10
COX7A2	Cytochrome c oxidase subunit 7A2	−0.45 ± 0.16	−0.87 ± 0.14	−0.56 ± 0.07
UQCRFS1	Cytochrome *b*-c1 subunit Rieske	−0.26 ± 0.23	−0.99 ± 0.16	−0.60 ± 0.08
UQCRQ	Cytochrome *b*-c1 complex subunit 8	−0.78 ± 0.17	−1.12 ± 0.12	−1.65 ± 0.28
GPD2	Glycerol-3-phosphate dehydrogenase	−1.06 ± 0.17	−1.36 ± 0.14	−1.76 ± 0.08
MAOB	Amine oxidase [flavin-containing] B	−1.38 ± 0.16	−2.10 ± 0.22	−2.55 ± 0.14
NDUFB3	NADH dehydrogenase 1 beta subunit 3	−0.22 ± 0.06	−0.28 ± 0.09	−0.59 ± 0.05
PRDX3	Peroxide reductase	−0.06 ± 0.09	−0.74 ± 0.10	−0.52 ± 0.13
SOD2	Superoxide dismutase [Mn]	−0.59 ± 0.05	−0.80 ± 0.06	−0.65 ± 0.05
Protein Synthesis				
EIF3C	EIF 3 subunit C	0.63 ± 0.04	0.46 ± 0.03	0.44 ± 0.05
EIF3E	EIF 3 subunit E	0.60 ± 0.06	0.56 ± 0.05	0.60 ± 0.07
KHSRP	Far upstream element-binding protein 2	0.16 ± 0.12	0.53 ± 0.05	0.59 ± 0.07
RPL5	60S ribosomal protein L5	0.60 ± 0.11	0.29 ± 0.06	0.43 ± 0.06
RRBP1	Ribosome-binding protein 1	1.06 ± 0.12	1.03 ± 0.11	0.78 ± 0.09
RPS19	40S ribosomal protein S19	0.60 ± 0.05	0.27 ± 0.05	0.39 ± 0.08
DARS	Aspartyl-tRNA synthetase, cytoplasmic	0.62 ± 0.02	0.45 ± 0.10	0.55 ± 0.09
Protein Folding and Transport				
ERP29	ER resident protein 29	0.82 ± 0.04	0.32 ± 0.05	0.20 ± 0.06
LMAN1	Protein ERGIC-53	0.75 ± 0.07	0.62 ± 0.04	0.65 ± 0.03
MOGS	Mannosyl-oligosaccharide glucosidase	1.15 ± 0.05	1.16 ± 0.10	0.80 ± 0.14
PDIA6	Protein disulfide-isomerase A6	1.04 ± 0.09	0.61 ± 0.09	0.48 ± 0.11
MIA3	Melanoma inhibitory activity protein 3	1.13 ± 0.08	0.97 ± 0.08	0.90 ± 0.12
NME2	Nucleoside diphosphate kinase B	0.64 ± 0.05	0.19 ± 0.16	0.50 ± 0.06
ARCN1	Coatomer subunit delta	0.81 ± 0.006	0.65 ± 0.04	0.56 ± 0.05
COPA	Coatomer subunit alpha	0.76 ± 0.03	0.70 ± 0.04	0.56 ± 0.05
SEC23A	Protein transport protein Sec23A	0.57 ± 0.08	0.66 ± 0.05	0.64 ± 0.02
Processing and Hormone Secretion				
GCG	Glucagon	−1.14 ± 0.29	−1.50 ± 0.06	−1.23 ± 0.07
PCSK1	Neuroendocrine convertase 1	−1.03 ± 0.20	−0.74 ± 0.24	−0.35 ± 0.14
PCSK2	Neuroendocrine convertase 2	−1.11 ± 0.15	−0.21 ± 0.28	−0.16 ± 0.17
PYY	Peptide YY	−1.35 ± 0.37	−1.30 ± 0.07	−0.93 ± 0.1
RTN4	Reticulon-4	−1.05 ± 0.12	−1.27 ± 0.13	−1.23 ± 0.09
SST	Somatostatin	−1.58 ± 0.30	−2.32 ± 0.07	−2.42 ± 0.09
STXBP1	Syntaxin-binding protein 1	−0.47 ± 0.06	−0.83 ± 0.12	−0.91 ± 0.08
UCN3	Urocortin-3	−2.40 ± 0.14	−1.47 ± 0.32	−1.19 ± 0.27
VAMP2	Vesicle-associated membrane protein 2	−0.91 ± 0.14	−0.28 ± 0.14	−0.05 ± 0.1
Antiapoptosis				
TXNDC5	Thioredoxin domain-containing protein 5	1.23 ± 0.08	0.95 ± 0.10	0.75 ± 0.11
TPT1	Translationally controlled tumor protein	0.85 ± 0.06	0.82 ± 0.07	0.60 ± 0.12

DOI: 10.1021/acs.jproteome.5b00587
J. Proteome Res. 2015, 14, 3111−3122

Table 1. continued

gene symbol	protein name	log$_2$ ratio ± SEM		
		HFD vs control	ob/ob (S) vs control	ob/ob (L) vs control
Antiapoptosis				
HSPA5	78 kDa glucose-regulated protein	0.82 ± 0.06	0.57 ± 0.09	0.55 ± 0.08
HSP90B1	Endoplasmin	0.67 ± 0.08	0.18 ± 0.08	0.06 ± 0.11
TMX1	Thioredoxin-related membrane protein 1	0.85 ± 0.08	0.52 ± 0.15	0.25 ± 0.16
ANXA4	Annexin A4	0.15 ± 0.03	0.53 ± 0.06	0.70 ± 0.05
Proapoptosis				
HSPD1	60 kDa heat shock protein, mitochondrial	−0.46 ± 0.06	−0.56 ± 0.07	−0.69 ± 0.03
HSPA9	Stress-70 protein, mitochondrial	−0.63 ± 0.10	−0.66 ± 0.06	−0.84 ± 0.03
RTN4	Reticulon-4	−1.05 ± 0.12	−1.27 ± 0.13	−1.23 ± 0.09
Proliferation				
CDK5rap3	CDK5 regulatory subunit-associated protein	0.83 ± 0.14	0.65 ± 0.09	0.60 ± 0.09
PRDX6	Peroxiredoxin-6	0.43 ± 0.04	0.65 ± 0.05	0.74 ± 0.02
Sel1l	Protein sel-1 homologue 1	1.35 ± 0.10	1.55 ± 0.18	1.61 ± 0.16
Nucb2	Nucleobindin-2	1.13 ± 0.11	1.14 ± 0.08	1.18 ± 0.08
SEPT5	Septin-5	1.34 ± 0.12	1.75 ± 0.07	1.54 ± 0.08
SEPT7	Septin-7	0.34 ± 0.06	0.44 ± 0.06	0.71 ± 0.05
NPM	Nucleophosmin	0.40 ± 0.07	0.68 ± 0.10	0.45 ± 0.07

[a]All changes are presented as log$_2$ ratio between HFD or ob/ob versus control. Standard errors of the mean (SEM) for log$_2$ ratio are also included. Proteins are grouped by functional analysis results using Ingenuity Pathway Analysis (IPA).

enzyme of defense against oxidative damage, to be downregulated in all insulin-resistant islets

Protein Synthesis and Transport and Endoplasmic Reticulum Stress

A remarkable feature observed in this study is the upregulation of key components of the translational machinery (Table 1 and Supporting Information Table S2). Eukaryotic translation initiation factors (eIFs), such as eIF3C, eIF3E, eIF3F, eIF3G, eIF3H, eIF2S1, and subsets of ribosomal proteins including RPL5, RPL7, and RPS19 were upregulated, and several proteins implicated in biogenesis of ribosomal and/or tRNAs, such as keratin 7 (KRT7), nucleophosmin (NMP1), ribosomal binding protein 1 (RRBP1), aspartyl-tRNA synthetase (DARS), and phenylalanyl-tRNA synthetase beta subunit (FARSB), were found to be overexpressed in islets from HFD and ob/ob islets as compared to control islets. ER stress proteins, including endoplasmic proteins 29 and 44 (ERP29 and ER44), lectin mannose-binding 1 (LMAN1), mannosyl-oligosaccharide glucosidase (MOGS), protein disulfide isomerase family A, members 3 and 6 (PDIA3 and PDIA6), and selenoprotein 15 (SEP15) were upregulated in insulin-resistant islets. Significant upregulation of key proteins implicated in facilitating intracellular protein transport was also observed, including endoplasmic reticulum protein 29 (ERP29), eukaryotic initiation factor 5A (EIF5A), melanoma inhibitory activity 3 (MIA3), new molecular entity 2 (NME2), nucleophosmin (NPM1), protein disulfide isomerase 3 (PDIA3), and SEC23-interacting protein (SEC23IP). Additionally, several members of clathrin-ordered proteins family (COP) involved in protein transport and cell membrane organization manifested substantial increases in their protein levels in insulin-resistant islets.

Insulin Processing and Exocytosis

In contrast to the marked increase in the machinery of protein biosynthesis, folding, and transport, a substantial downregulation of proteins involved in hormone processing, PCSK1 and PCSK2,[24] was observed in both models of insulin resistance, although it was more pronounced in HFD islets. Consistent with the latter observation, glucagon and somatostatin were downregulated in islets derived from HFD and ob/ob mice. Finally, several proteins implicated in vesicular transport and exocytosis of hormone granules, such as VAMP2,[25] RAB5C, RAB7A, STYL4, and UCN3,[26] were also downregulated (Table 1 and Supporting Information Table S2).

Apoptosis and Proliferation

Increased β-cell mass in rodents is a major structural compensation to insulin resistance that involves both an enhancement of cell proliferation and inhibition of cell death.[7a,27] However, the downstream intracellular targets mediating these effects have not been fully identified. Using IPA analysis, we focused on identifying factors that are relevant to cell survival and proliferation. We observed that several anti-apoptotic factors, including TXNDC5, TPT1, HSPA5, HSP90B1, TXM1, and ANXA4, were found to be commonly upregulated, whereas proapoptotic factors, such as HSPDA1, HSPA9, and RTN4, are downregulated in islets derived from either HFD or ob/ob models. On the other hand, and in agreement with the compensatory role of cell proliferation in insulin-resistant islets, we found that several proliferation-linked proteins were upregulated in insulin-resistant islets, including isoform 1 of protein SEL-1 homolog1 (Sel1l), previously reported for its mitogenic action on β-cells.[28] We also found nucleobindin-2 (Nucb2),[29] CDK5 regulatory subunit associated protein 3 (CDK5rap3),[30] and peroxiredoxin 6 (PRDX6)[31] to be upregulated in both HFD and ob/ob islets, suggesting their potential in promoting proliferation of insulin-resistant islet cells. Moreover, a notable increase was observed in SEPT5 and SEPT7, members of the septin family known to control cell division,[32] and nucleophosmin-1 (NPM), a protein described to promote c-Myc-mediated proliferation[33] (Table 1).

Western Blot Validation of Selected Protein Targets

Considering that most islet proteome changes occur in both HFD and ob/ob models and in both small and large islets, we focused on the ob/ob mouse model to validate key regulated proteins in various biological processes in insulin-resistant states. To this end, we isolated islets from 5 month old wild-

DOI: 10.1021/acs.jproteome.5b00587
J. Proteome Res. 2015, 14, 3111−3122

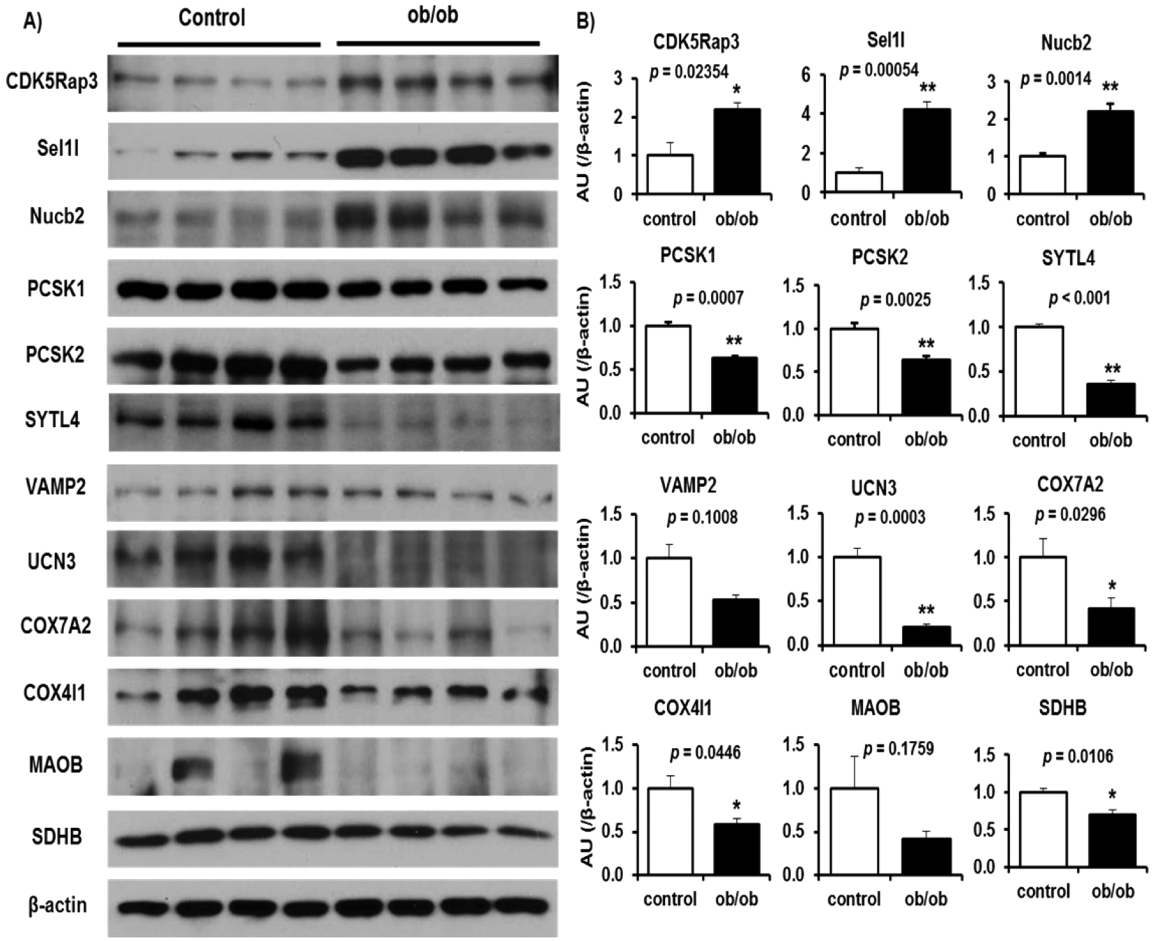

Figure 4. Validation of key regulated proteins in ob/ob mice. (A) The total cell extracts from the islets were subjected to immunoblotting as indicated. (B) Intensity of the signals quantified by densitometry (ImageJ) (n = 4–6). Data are normalized to actin. Individual p values from Student's t test for each quantification are indicated in (B).

type or age matched ob/ob mice and subjected the extracted proteins to western blotting and quantification (Figure 4A,B). Consistent with proteomics data, we observed that expression of CDK5rap3, Sel1I, and Nucb2, proteins reported to be linked to proliferation, are increased in ob/ob islets as compared to the control group. Moreover, expression of PCSK1 and PCSK2, involved in hormone biosynthesis, was downregulated in insulin-resistant ob/ob islets in western blot experiments, similar to the proteomics data. Additionally, a decrease in expression of SYTL4, UCN3, and VAMP2 exocytosis-regulating proteins was validated in ob/ob islets. A subset of proteins involved in mitochondrial function and oxidative phosphorylation, including COX4I1 and COX7A2, was also decreased, consistent with the proteomics data. Finally, we confirmed by western blot that two metabolic enzymes, MAOB and SDHB, are downregulated in ob/ob islets as compared to controls (Figure 4).

DISCUSSION

This study was designed to interrogate changes occurring in the islet proteome of insulin-resistant models prior to the development of overt diabetes. We used genetic leptin-deficient (ob/ob) and dietary-induced insulin resistance (HFD) mouse models to elucidate whether the compensatory islet cell response to insulin resistance is mediated by morphological or functional adaptation. Furthermore, we used small and large islets to uncover potentially distinct signatures in the adaptation of islet subpopulations to insulin resistance.

Surprisingly, most of the changes noted in our proteomic study were common between HFD and ob/ob, and only a subset of proteins appeared to be differentially regulated. One possibility for the observed similarities in the proteome phenotypes is that HFD mice develop leptin resistance in insulin-resistant settings[34] and become blind to the leptin as naturally occurring ob/ob mice. The alterations in proteins specific to HFD model were mainly involved in protein processing, translation, regulation of secretion, and exocytosis, whereas those specific to the ob/ob model were associated with processes such as sugar metabolism, oxidation and reduction processes, and chromatin and nucleosome assembly (Supporting Information Tables S4 and S5). These observations are intriguing and require further investigation.

A unique feature of our approach is the comparison between small and large islets in the ob/ob model. Although several previous studies have suggested functional differences in islet subpopulations in different species[35] that may occur in normal states, we observed that in the case of insulin resistance nearly all of the changes observed in proteins involved in hormone processing and secretory pathways, energy metabolism, mitochondrial function, protein synthesis, and ER stress were affected to a similar extent in both small and large islets in the ob/ob model. One interpretation of these data is that

DOI: 10.1021/acs.jproteome.5b00587
J. Proteome Res. 2015, 14, 3111–3122

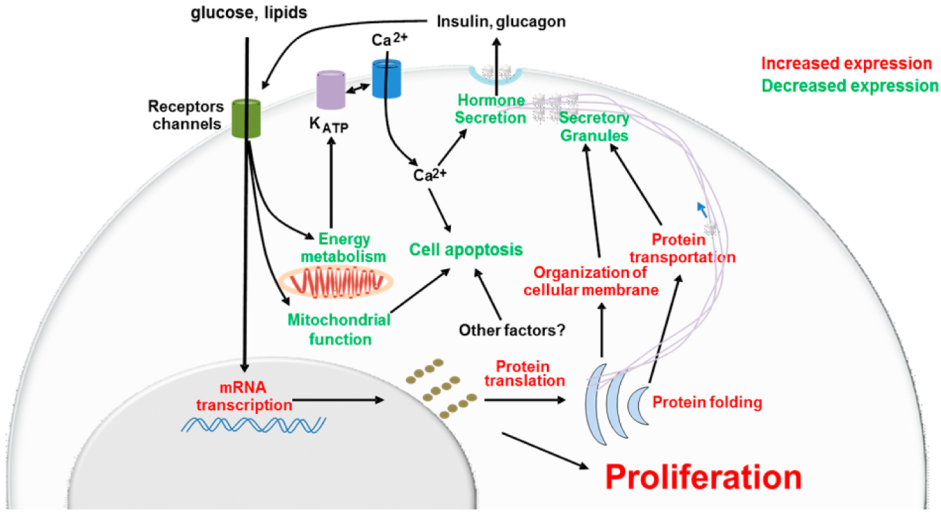

Figure 5. Islet compensatory response in insulin resistance: schematic illustrating major regulated pathways in insulin-resistant islets. Down- and upregulated biological processes are shown in green and red, respectively.

impairment of β-cell function likely precedes proliferation and that alterations in proliferation are unlikely to promote β-cell dysfunction. The cause of β-cell secretory dysfunction is likely due to a combination of the deleterious effects of hyperglycemia and hyperlipidemia and/or proinflammatory cytokines.[36] Consistently, several studies have reported alterations in function following chronic *in vitro* treatment of β-cells with glucose, FFA, or cytokines.[37]

In the global context, our data suggest that insulin-resistant conditions limit islet cell energy metabolism and shut down the ability of cells to produce sufficient amounts of key metabolic intermediates. This is illustrated by a decline in the abundance of proteins controlling various metabolic pathways, including glycolysis, Krebs cycle, amino acid metabolism, and mitochondrial oxidative phosphorylation. Moreover, several mitochondrial proteins were downregulated, suggesting mitochondrial dysfunction in islet cells derived from obese insulin-resistant animals. The reduction of antioxidant proteins, such as PRDX3 and SOD2, is suggestive of oxidative stress, consistent with the protective role of these proteins in islet cells, particularly in β-cells where the levels of these molecules are low, to mitigate oxidative stress.[38] However, islet cells showed increased PRDX6, another antioxidant member of the peroxiredoxin family known (as for PRDX3) to be downregulated by inflammation.[38b,39] It is possible that PRDX6 is upregulated by other stimulatory molecules to restore a mitochondrial redox state and protect the mice from developing overt diabetes.[40]

Several components of protein synthetic machinery, including proteins facilitating rRNA/tRNA biogenesis, initiation of translation factors, and regulators of protein transport and cell membrane organization, were found to be activated and potentially participating in enhancing the biosynthetic capacity of insulin and other hormones. Consistent with the latter possibility, ER overloading by newly synthesized proteins increased protein expression of ER stress-induced chaperones in an attempt to limit ER stress.

It is of interest that several proteins involved in oxidative metabolism that were decreased in islets from HFD or ob/ob islets were also reported to be downregulated in islets derived from 10 week old diabetic MKR mice.[9b] Commonly decreased proteins in HFD, ob/ob, and MKR models include PFKL, DLD, IDH1, COX5A, GPD2, and MAOB. Alterations in the expression of proteins in islets from models of prediabetes (e.g., HFD and ob/ob) that are also detectable in islets from diabetic MKR mice suggest their causal role in defective β-cell metabolism. We also observed that UCN3, a marker of β-cell maturation,[26,41] was decreased in HFD, ob/ob, and MKR models, consistent with its previously reported role in impaired glucose-stimulated insulin secretion.[42]

A previous study used differential islet proteome analyses of Zucker fatty (ZF) and Zucker diabetic fatty (ZDF) rats to reveal changes in the expression of proteins involved in insulin secretion, mitochondrial dysfunction, extracellular matrix proteins, or microvascular ischemia.[9a] Similar to the HFD or ob/ob models, islets derived from obese ZF rats also exhibited increased protein levels of ATP5l, COPB, NME2, or PGM2 and decreased levels of GCG, GOT2, IDH2, or PCSK1.[9a] This cross-species observation provides a valuable set of proteins associated with the transition from insulin resistance to type 2 diabetes in the context of islets. It is important, however, to note that some changes in the expression of secretory proteins, such as SCG2, RAB5C, and RAB7A, were commonly found in ZF or ZDF rats but not in HFD or ob/ob,[9a] suggesting that regulation of the expression of proteins involved in hormone secretion is not conserved in the mouse and rat.

As expected, several proteins involved in cell proliferation were increased in insulin-resistant islets.[43] We observed that the ER membrane protein suppressor of lin-12-like protein 1 (Sel1l) is upregulated in insulin-resistant islets. Sel1l is the ortholog of *Caenorhabditis elegans* gene sel-1, which is a negative regulator of LIN-12/NOTCH receptor proteins, previously implicated in β-cell growth and function. Heterozygote Sel1l ($\pm$) mice exhibit decreased β-cell mass due to reduced β-cell proliferation and are predisposed to hyperglycemia upon a high-fat diet.[28,44] Our observation of a substantial increase in the amount of CDK5rap3 in hyperplastic islets is interesting in the context of recent findings that overexpression of CDK5rap3 is positively correlated with cell proliferation of hepatocytes[30] and lung cells,[45] both of which, along with pancreatic cells, share a common endodermal origin. The increased expression of Nucb2, a protein reported to be expressed in human and rodent islet β-cells and shown to be decreased in islets derived from type 2 diabetic patients,[29b] is relevant because Nucb2 was reported to enhance cell

DOI: 10.1021/acs.jproteome.5b00587
J. Proteome Res. 2015, 14, 3111−3122

proliferation via EGF-stimulated MAPK kinase/Erk signaling.[46] The decreased islet levels of Nucb2 in patients with type 2 diabetes[29b] warrant studies to explore a role for this protein to enhance pancreatic β-cell proliferation. The increased amount of EIF5A in insulin-resistant compared to control islets in our studies suggests that this protein, which was initially described as an initiator of translation, may be also relevant in proliferation. For example, EGF stimulates proliferation of corneal epithelial cells through the PI3K−Akt−EIF5A signaling pathway,[47] and knockdown of EIF5A by small interfering RNAs abolishes the stimulatory action of EGF on cell proliferation.[47]

In summary, during the progression of insulin resistance, the secretory capacity of islet cells tends to decline upon downregulation of key proteins controlling multiple steps of insulin synthesis and release, including energy metabolism, mitochondrial function, and hormone biosynthesis/exocytosis. Increased cell survival and proliferation of the endocrine pancreas appear to be central features that enable islet cells to meet the chronic elevated demands for insulin and potentially other hormones (Figure 5). The candidates identified and validated in this article could be considered for strategies aimed at developing new antidiabetic therapeutics to enhance β-cell mass in efforts to counter diabetes.

■ ASSOCIATED CONTENT

Supporting Information

Table S1: List of all quantified proteins. All values in each sample are $\log_2$ of peptide intensities after normalization. Table S2: List of proteins showing significant change. All ratios are in $\log_2$ scale. Table S3: SRM validation of candidate proteins. Table S4: Protein candidates only showing significant change in HFD model. Table S5: Protein candidates only showing significant change in ob/ob model. Table S6: List of all identified peptides. Table S7: List of all SRM peptides and associated transitions. Figure S1: Histograms of the extent of changes for altered proteins. Figure S2: Examples of extracted ion chromatograms of SRM measurements.The Supporting Information is available free of charge on the ACS Publications website at DOI: 10.1021/acs.jproteome.5b00587.

■ AUTHOR INFORMATION

Corresponding Authors

*(W.-J.Q.) E-mail: weijun.qian@pnnl.gov; Tel: (509) 371-6572.

*(R.N.K.) E-mail: rohit.kulkarni@joslin.harvard.edu; Tel: (617) 309-3460.

Author Contributions

‖A.E., J.-Y.Z., and C.W.L. contributed equally to this work.

Author Contributions

⊥J.S. and E.D. contributed equally to this work.

Notes

The authors declare no competing financial interest.

■ ACKNOWLEDGMENTS

This work was supported by NIH grant nos. R01 DK074795, R01 DK067536, R01 DK103215, and K99 DK090210, Société Francophone du Diabète (to A.E.), Association Française des Diabétiques (to A.E.), American Diabetes Association (to A.E.), and JDRF advanced postdoctoral fellowship (to A.E.). Samples were analyzed using capabilities developed under the support of the NIH Biomedical Technology Research Resource for integrative biology (P41 GM103493). Significant portions of the work were performed in the Environmental Molecular Science Laboratory, a DOE/BER national scientific user facility at Pacific Northwest National Laboratory (PNNL) in Richland, Washington. PNNL is operated for the DOE by Battelle under contract no. DE-AC05-76RLO-1830.

■ REFERENCES

(1) (a) Assmann, A.; Hinault, C.; Kulkarni, R. N. Growth factor control of pancreatic islet regeneration and function. *Pediatr. Diabetes* **2009**, *10* (1), 14−32. (b) Weir, G. C.; Bonner-Weir, S. Five stages of evolving beta-cell dysfunction during progression to diabetes. *Diabetes* **2004**, *53* (Suppl3), S16−S21.

(2) Wild, S.; Roglic, G.; Green, A.; Sicree, R.; King, H. Global prevalence of diabetes: estimates for the year 2000 and projections for 2030. *Diabetes Care* **2004**, *27*, 1047−53.

(3) Doria, A.; Patti, M. E.; Kahn, C. R. The emerging genetic architecture of type 2 diabetes. *Cell Metab.* **2008**, *8*, 186−200.

(4) (a) Shapiro, A. M.; Ricordi, C.; Hering, B. J.; Auchincloss, H.; Lindblad, R.; Robertson, R. P.; Secchi, A.; Brendel, M. D.; Berney, T.; Brennan, D. C.; Cagliero, E.; Alejandro, R.; Ryan, E. A.; DiMercurio, B.; Morel, P.; Polonsky, K. S.; Reems, J. A.; Bretzel, R. G.; Bertuzzi, F.; Froud, T.; Kandaswamy, R.; Sutherland, D. E.; Eisenbarth, G.; Segal, M.; Preiksaitis, J.; Korbutt, G. S.; Barton, F. B.; Viviano, L.; Seyfert-Margolis, V.; Bluestone, J.; Lakey, J. R. International trial of the Edmonton protocol for islet transplantation. *N. Engl. J. Med.* **2006**, *355*, 1318−30. (b) Thompson, D. M.; Meloche, M.; Ao, Z.; Paty, B.; Keown, P.; Shapiro, R. J.; Ho, S.; Worsley, D.; Fung, M.; Meneilly, G.; Begg, I.; Al Mehthel, M.; Kondi, J.; Harris, C.; Fensom, B.; Kozak, S. E.; Tong, S. O.; Trinh, M.; Warnock, G. L. Reduced progression of diabetic microvascular complications with islet cell transplantation compared with intensive medical therapy. *Transplantation* **2011**, *91*, 373−8.

(5) (a) Buteau, J.; Shlien, A.; Foisy, S.; Accili, D. Metabolic diapause in pancreatic beta-cells expressing a gain-of-function mutant of the forkhead protein Foxo1. *J. Biol. Chem.* **2007**, *282*, 287−93. (b) de Koning, E. J.; Bonner-Weir, S.; Rabelink, T. J. Preservation of beta-cell function by targeting beta-cell mass. *Trends Pharmacol. Sci.* **2008**, *29*, 218−27. (c) Hansen, J. B.; Arkhammar, P. O.; Bodvarsdottir, T. B.; Wahl, P. Inhibition of insulin secretion as a new drug target in the treatment of metabolic disorders. *Curr. Med. Chem.* **2004**, *11*, 1595−615. (d) Talchai, C.; Xuan, S.; Lin, H. V.; Sussel, L.; Accili, D. Pancreatic beta cell dedifferentiation as a mechanism of diabetic beta cell failure. *Cell* **2012**, *150*, 1223−34.

(6) (a) Jones, C. N.; Pei, D.; Staris, P.; Polonsky, K. S.; Chen, Y. D.; Reaven, G. M. Alterations in the glucose-stimulated insulin secretory dose-response curve and in insulin clearance in nondiabetic insulin-resistant individuals. *J. Clin. Endocrinol. Metab.* **1997**, *82*, 1834−8. (b) Parsons, J. A.; Brelje, T. C.; Sorenson, R. L. Adaptation of islets of Langerhans to pregnancy: increased islet cell proliferation and insulin secretion correlates with the onset of placental lactogen secretion. *Endocrinology* **1992**, *130*, 1459−66. (c) Polonsky, K. S.; Given, B. D.; Hirsch, L.; Shapiro, E. T.; Tillil, H.; Beebe, C.; Galloway, J. A.; Frank, B. H.; Karrison, T.; Van Cauter, E. Quantitative study of insulin secretion and clearance in normal and obese subjects. *J. Clin. Invest.* **1988**, *81*, 435−41.

(7) (a) Bruning, J. C.; Winnay, J.; Bonner-Weir, S.; Taylor, S. I.; Accili, D.; Kahn, C. R. Development of a novel polygenic model of NIDDM in mice heterozygous for IR and IRS-1 null alleles. *Cell* **1997**, *88*, 561−72. (b) Michael, M. D.; Kulkarni, R. N.; Postic, C.; Previs, S. F.; Shulman, G. I.; Magnuson, M. A.; Kahn, C. R. Loss of insulin signaling in hepatocytes leads to severe insulin resistance and progressive hepatic dysfunction. *Mol. Cell* **2000**, *6*, 87−97.

(8) (a) Chen, C.; Hosokawa, H.; Bumbalo, L. M.; Leahy, J. L. Mechanism of compensatory hyperinsulinemia in normoglycemic insulin-resistant spontaneously hypertensive rats. Augmented enzymatic activity of glucokinase in beta-cells. *J. Clin. Invest.* **1994**, *94*, 399−404. (b) Liu, Y. Q.; Jetton, T. L.; Leahy, J. L. beta-Cell adaptation to

DOI: 10.1021/acs.jproteome.5b00587
J. Proteome Res. 2015, 14, 3111−3122

insulin resistance. Increased pyruvate carboxylase and malate-pyruvate shuttle activity in islets of nondiabetic Zucker fatty rats. *J. Biol. Chem.* **2002**, *277*, 39163−8.

(9) (a) Han, D.; Moon, S.; Kim, H.; Choi, S. E.; Lee, S. J.; Park, K. S.; Jun, H.; Kang, Y.; Kim, Y. Detection of differential proteomes associated with the development of type 2 diabetes in the Zucker rat model using the iTRAQ technique. *J. Proteome Res.* **2011**, *10*, 564−77. (b) Lu, H.; Koshkin, V.; Allister, E. M.; Gyulkhandanyan, A. V.; Wheeler, M. B. Molecular and metabolic evidence for mitochondrial defects associated with beta-cell dysfunction in a mouse model of type 2 diabetes. *Diabetes* **2010**, *59*, 448−59. (c) Lu, H.; Yang, Y.; Allister, E. M.; Wijesekara, N.; Wheeler, M. B. The identification of potential factors associated with the development of type 2 diabetes: a quantitative proteomics approach. *Mol. Cell. Proteomics* **2008**, *7*, 1434−51. (d) Qiu, L.; List, E. O.; Kopchick, J. J. Differentially expressed proteins in the pancreas of diet-induced diabetic mice. *Mol. Cell. Proteomics* **2005**, *4*, 1311−8.

(10) Perez-Vazquez, V.; Guzman-Flores, J. M.; Mares-Alvarez, D.; Hernandez-Ortiz, M.; Macias-Cervantes, M. H.; Ramirez-Emiliano, J.; Encarnacion-Guevara, S. Differential proteomic analysis of the pancreas of diabetic db/db mice reveals the proteins involved in the development of complications of diabetes mellitus. *Int. J. Mol. Sci.* **2014**, *15*, 9579−93.

(11) Kulkarni, R. N.; Bruning, J. C.; Winnay, J. N.; Postic, C.; Magnuson, M. A.; Kahn, C. R. Tissue-specific knockout of the insulin receptor in pancreatic beta cells creates an insulin secretory defect similar to that in type 2 diabetes. *Cell* **1999**, *96*, 329−39.

(12) Kulkarni, R. N.; Winnay, J. N.; Daniels, M.; Bruning, J. C.; Flier, S. N.; Hanahan, D.; Kahn, C. R. Altered function of insulin receptor substrate-1-deficient mouse islets and cultured beta-cell lines. *J. Clin. Invest.* **1999**, *104*, R69−75.

(13) Wang, H.; Qian, W. J.; Mottaz, H. M.; Clauss, T. R.; Anderson, D. J.; Moore, R. J.; Camp, D. G., 2nd; Khan, A. H.; Sforza, D. M.; Pallavicini, M.; Smith, D. J.; Smith, R. D. Development and evaluation of a micro- and nanoscale proteomic sample preparation method. *J. Proteome Res.* **2005**, *4*, 2397−403.

(14) Zhou, J. Y.; Schepmoes, A. A.; Zhang, X.; Moore, R. J.; Monroe, M. E.; Lee, J. H.; Camp, D. G.; Smith, R. D.; Qian, W. J. Improved LC-MS/MS spectral counting statistics by recovering low-scoring spectra matched to confidently identified peptide sequences. *J. Proteome Res.* **2010**, *9*, 5698−704.

(15) Kim, S.; Gupta, N.; Pevzner, P. A. Spectral probabilities and generating functions of tandem mass spectra: a strike against decoy databases. *J. Proteome Res.* **2008**, *7*, 3354−63.

(16) Nesvizhskii, A. I.; Keller, A.; Kolker, E.; Aebersold, R. A statistical model for identifying proteins by tandem mass spectrometry. *Anal. Chem.* **2003**, *75*, 4646−58.

(17) Elias, J. E.; Gygi, S. P. Target-decoy search strategy for increased confidence in large-scale protein identifications by mass spectrometry. *Nat. Methods* **2007**, *4*, 207−14.

(18) (a) Qian, W. J.; Liu, T.; Petyuk, V. A.; Gritsenko, M. A.; Petritis, B. O.; Polpitiya, A. D.; Kaushal, A.; Xiao, W.; Finnerty, C. C.; Jeschke, M. G.; Jaitly, N.; Monroe, M. E.; Moore, R. J.; Moldawer, L. L.; Davis, R. W.; Tompkins, R. G.; Herndon, D. N.; Camp, D. G.; Smith, R. D. Large-scale multiplexed quantitative discovery proteomics enabled by the use of an (18)O-labeled "universal" reference sample. *J. Proteome Res.* **2009**, *8*, 290−9. (b) Zimmer, J. S.; Monroe, M. E.; Qian, W. J.; Smith, R. D. Advances in proteomics data analysis and display using an accurate mass and time tag approach. *Mass Spectrom. Rev.* **2006**, *25*, 450−82.

(19) Monroe, M. E.; Tolic, N.; Jaitly, N.; Shaw, J. L.; Adkins, J. N.; Smith, R. D. VIPER: an advanced software package to support high-throughput LC-MS peptide identification. *Bioinformatics* **2007**, *23*, 2021−3.

(20) Polpitiya, A. D.; Qian, W. J.; Jaitly, N.; Petyuk, V. A.; Adkins, J. N.; Camp, D. G.; Anderson, G. A.; Smith, R. D. DAnTE: a statistical tool for quantitative analysis of -omics data. *Bioinformatics* **2008**, *24*, 1556−1558.

(21) Petritis, B. O.; Qian, W. J.; Camp, D. G., 2nd; Smith, R. D. A simple procedure for effective quenching of trypsin activity and prevention of 18O-labeling back-exchange. *J. Proteome Res.* **2009**, *8*, 2157−63.

(22) Kim, J. S.; Fillmore, T. L.; Liu, T.; Robinson, E.; Hossain, M.; Champion, B. L.; Moore, R. J.; Camp, D. G., 2nd; Smith, R. D.; Qian, W. J. 18O-labeled proteome reference as global internal standards for targeted quantification by selected reaction monitoring-mass spectrometry. *Mol. Cell. Proteomics* **2011**, *10*, M110.007302.

(23) (a) Shi, T.; Fillmore, T. L.; Sun, X.; Zhao, R.; Schepmoes, A. A.; Hossain, M.; Xie, F.; Wu, S.; Kim, J. S.; Jones, N.; Moore, R. J.; Pasa-Tolic, L.; Kagan, J.; Rodland, K. D.; Liu, T.; Tang, K.; Camp, D. G., 2nd; Smith, R. D.; Qian, W. J. Antibody-free, targeted mass-spectrometric approach for quantification of proteins at low picogram per milliliter levels in human plasma/serum. *Proc. Natl. Acad. Sci. U. S. A.* **2012**, *109*, 15395−400. (b) Shi, T.; Qian, W. J. Antibody-free PRISM-SRM for multiplexed protein quantification: is this the new competition for immunoassays in bioanalysis? *Bioanalysis* **2013**, *5*, 267−9.

(24) Neerman-Arbez, M.; Cirulli, V.; Halban, P. A. Levels of the conversion endoproteases PC1 (PC3) and PC2 distinguish between insulin-producing pancreatic islet beta cells and non-beta cells. *Biochem. J.* **1994**, *300*, 57−61.

(25) Regazzi, R.; Sadoul, K.; Meda, P.; Kelly, R. B.; Halban, P. A.; Wollheim, C. B. Mutational analysis of VAMP domains implicated in Ca^{2+}-induced insulin exocytosis. *EMBO J.* **1996**, *15*, 6951−9.

(26) Blum, B.; Hrvatin, S. S.; Schuetz, C.; Bonal, C.; Rezania, A.; Melton, D. A. Functional beta-cell maturation is marked by an increased glucose threshold and by expression of urocortin 3. *Nat. Biotechnol.* **2012**, *30*, 261−4.

(27) (a) Chen, Z.; Morris, D. L.; Jiang, L.; Liu, Y.; Rui, L. SH2B1 in beta cells regulates glucose metabolism by promoting beta cell survival and islet expansion. *Diabetes* **2014**, *63*, 585−95. (b) Jetton, T. L.; Lausier, J.; LaRock, K.; Trotman, W. E.; Larmie, B.; Habibovic, A.; Peshavaria, M.; Leahy, J. L. Mechanisms of compensatory beta-cell growth in insulin-resistant rats: roles of Akt kinase. *Diabetes* **2005**, *54*, 2294−304. (c) Okada, T.; Liew, C. W.; Hu, J.; Hinault, C.; Michael, M. D.; Krtzfeldt, J.; Yin, C.; Holzenberger, M.; Stoffel, M.; Kulkarni, R. N. Insulin receptors in beta-cells are critical for islet compensatory growth response to insulin resistance. *Proc. Natl. Acad. Sci. U. S. A.* **2007**, *104*, 8977−82.

(28) Francisco, A. B.; Singh, R.; Sha, H.; Yan, X.; Qi, L.; Lei, X.; Long, Q. Haploid insufficiency of suppressor enhancer Lin12 1-like (SEL1L) protein predisposes mice to high fat diet-induced hyperglycemia. *J. Biol. Chem.* **2011**, *286*, 22275−82.

(29) (a) Oh, I. S.; Shimizu, H.; Satoh, T.; Okada, S.; Adachi, S.; Inoue, K.; Eguchi, H.; Yamamoto, M.; Imaki, T.; Hashimoto, K.; Tsuchiya, T.; Monden, T.; Horiguchi, K.; Yamada, M.; Mori, M. Identification of nesfatin-1 as a satiety molecule in the hypothalamus. *Nature* **2006**, *443*, 709−12. (b) Riva, M.; Nitert, M. D.; Voss, U.; Sathanoori, R.; Lindqvist, A.; Ling, C.; Wierup, N. Nesfatin-1 stimulates glucagon and insulin secretion and beta cell NUCB2 is reduced in human type 2 diabetic subjects. *Cell Tissue Res.* **2011**, *346*, 393−405.

(30) Mak, G. W.; Chan, M. M.; Leong, V. Y.; Lee, J. M.; Yau, T. O.; Ng, I. O.; Ching, Y. P. Overexpression of a novel activator of PAK4, the CDK5 kinase-associated protein CDK5RAP3, promotes hepatocellular carcinoma metastasis. *Cancer Res.* **2011**, *71*, 2949−58.

(31) Chang, X. Z.; Li, D. Q.; Hou, Y. F.; Wu, J.; Lu, J. S.; Di, G. H.; Jin, W.; Ou, Z. L.; Shen, Z. Z.; Shao, Z. M. Identification of the functional role of peroxiredoxin 6 in the progression of breast cancer. *Breast cancer research: BCR* **2007**, *9*, R76.

(32) Mostowy, S.; Cossart, P. Septins: the fourth component of the cytoskeleton. *Nat. Rev. Mol. Cell Biol.* **2012**, *13*, 183−94.

(33) Li, Z.; Hann, S. R. Nucleophosmin is essential for c-Myc nucleolar localization and c-Myc-mediated rDNA transcription. *Oncogene* **2013**, *32*, 1988−94.

(34) Enriori, P. J.; Evans, A. E.; Sinnayah, P.; Jobst, E. E.; Tonelli-Lemos, L.; Billes, S. K.; Glavas, M. M.; Grayson, B. E.; Perello, M.;

DOI: 10.1021/acs.jproteome.5b00587
J. Proteome Res. 2015, 14, 3111−3122

Nillni, E. A.; Grove, K. L.; Cowley, M. A. Diet-induced obesity causes severe but reversible leptin resistance in arcuate melanocortin neurons. *Cell Metab.* **2007**, *5*, 181−94.
(35) (a) Bonner-Weir, S.; Like, A. A. A dual population of islets of Langerhans in bovine pancreas. *Cell Tissue Res.* **1980**, *206*, 157−70. (b) Farhat, B.; Almelkar, A.; Ramachandran, K.; Williams, S. J.; Huang, H. H.; Zamierowksi, D.; Novikova, L.; Stehno-Bittel, L. Small human islets comprised of more beta-cells with higher insulin content than large islets. *Islets* **2013**, *5*, 87−94. (c) Huang, H. H.; Novikova, L.; Williams, S. J.; Smirnova, I. V.; Stehno-Bittel, L. Low insulin content of large islet population is present in situ and in isolated islets. *Islets* **2011**, *3*, 6−13.
(36) Robertson, R. P. Beta-cell deterioration during diabetes: what's in the gun? *Trends Endocrinol. Metab.* **2009**, *20*, 388−93.
(37) (a) Chen, X.; Cui, Z.; Wei, S.; Hou, J.; Xie, Z.; Peng, X.; Li, J.; Cai, T.; Hang, H.; Yang, F. Chronic high glucose induced INS-1beta cell mitochondrial dysfunction: a comparative mitochondrial proteome with SILAC. *Proteomics* **2013**, *13*, 3030−9. (b) D'Hertog, W.; Overbergh, L.; Lage, K.; Ferreira, G. B.; Maris, M.; Gysemans, C.; Flamez, D.; Cardozo, A. K.; Van den Bergh, G.; Schoofs, L.; Arckens, L.; Moreau, Y.; Hansen, D. A.; Eizirik, D. L.; Waelkens, E.; Mathieu, C. Proteomics analysis of cytokine-induced dysfunction and death in insulin-producing INS-1E cells: new insights into the pathways involved. *Mol. Cell. Proteomics* **2007**, *6*, 2180−99. (c) Maris, M.; Ferreira, G. B.; D'Hertog, W.; Cnop, M.; Waelkens, E.; Overbergh, L.; Mathieu, C. High glucose induces dysfunction in insulin secretory cells by different pathways: a proteomic approach. *J. Proteome Res.* **2010**, *9*, 6274−87. (d) Maris, M.; Robert, S.; Waelkens, E.; Derua, R.; Hernangomez, M. H.; D'Hertog, W.; Cnop, M.; Mathieu, C.; Overbergh, L. Role of the saturated nonesterified fatty acid palmitate in beta cell dysfunction. *J. Proteome Res.* **2013**, *12*, 347−62.
(38) (a) Kang, L.; Dai, C.; Lustig, M. E.; Bonner, J. S.; Mayes, W. H.; Mokshagundam, S.; James, F. D.; Thompson, C. S.; Lin, C. T.; Perry, C. G.; Anderson, E. J.; Neufer, P. D.; Wasserman, D. H.; Powers, A. C. Heterozygous SOD2 deletion impairs glucose-stimulated insulin secretion, but not insulin action, in high-fat-fed mice. *Diabetes* **2014**, *63*, 3699−710. (b) Wolf, G.; Aumann, N.; Michalska, M.; Bast, A.; Sonnemann, J.; Beck, J. F.; Lendeckel, U.; Newsholme, P.; Walther, R. Peroxiredoxin III protects pancreatic ss cells from apoptosis. *J. Endocrinol.* **2010**, *207*, 163−75.
(39) Paula, F. M.; Ferreira, S. M.; Boschero, A. C.; Souza, K. L. Modulation of the peroxiredoxin system by cytokines in insulin-producing RINm5F cells: down-regulation of PRDX6 increases susceptibility of beta cells to oxidative stress. *Mol. Cell. Endocrinol.* **2013**, *374*, 56−64.
(40) Pacifici, F.; Arriga, R.; Sorice, G. P.; Capuani, B.; Scioli, M. G.; Pastore, D.; Donadel, G.; Bellia, A.; Caratelli, S.; Coppola, A.; Ferrelli, F.; Federici, M.; Sconocchia, G.; Tesauro, M.; Sbraccia, P.; Della-Morte, D.; Giaccari, A.; Orlandi, A.; Lauro, D. Peroxiredoxin 6, a novel player in the pathogenesis of diabetes. *Diabetes* **2014**, *63*, 3210−20.
(41) van der Meulen, T.; Xie, R.; Kelly, O. G.; Vale, W. W.; Sander, M.; Huising, M. O. Urocortin 3 marks mature human primary and embryonic stem cell-derived pancreatic alpha and beta cells. *PLoS One* **2012**, *7*, e52181.
(42) Li, C.; Chen, P.; Vaughan, J.; Lee, K. F.; Vale, W. Urocortin 3 regulates glucose-stimulated insulin secretion and energy homeostasis. *Proc. Natl. Acad. Sci. U. S. A.* **2007**, *104*, 4206−11.
(43) (a) Bock, T.; Pakkenberg, B.; Buschard, K. Increased islet volume but unchanged islet number in ob/ob mice. *Diabetes* **2003**, *52*, 1716−22. (b) Hull, R. L.; Kodama, K.; Utzschneider, K. M.; Carr, D. B.; Prigeon, R. L.; Kahn, S. E. Dietary-fat-induced obesity in mice results in beta cell hyperplasia but not increased insulin release: evidence for specificity of impaired beta cell adaptation. *Diabetologia* **2005**, *48*, 1350−8. (c) Stamateris, R. E.; Sharma, R. B.; Hollern, D. A.; Alonso, L. C. Adaptive beta-cell proliferation increases early in high-fat feeding in mice, concurrent with metabolic changes, with induction of islet cyclin D2 expression. *Am. J. Physiol Endocrinol Metab* **2013**, *305*, E149−59.
(44) Sun, S.; Shi, G.; Han, X.; Francisco, A. B.; Ji, Y.; Mendonca, N.; Liu, X.; Locasale, J. W.; Simpson, K. W.; Duhamel, G. E.; Kersten, S.; Yates, J. R., 3rd; Long, Q.; Qi, L. Sel1L is indispensable for mammalian endoplasmic reticulum-associated degradation, endoplasmic reticulum homeostasis, and survival. *Proc. Natl. Acad. Sci. U. S. A.* **2014**, *111*, E582−91.
(45) Stav, D.; Bar, I.; Sandbank, J. Usefulness of CDK5RAP3, CCNB2, and RAGE genes for the diagnosis of lung adenocarcinoma. *IInt. J. Biol. Markers* **2007**, *22*, 108−13.
(46) Tagaya, Y.; Miura, A.; Okada, S.; Ohshima, K.; Mori, M. Nucleobindin-2 is a positive modulator of EGF-dependent signals leading to enhancement of cell growth and suppression of adipocyte differentiation. *Endocrinology* **2012**, *153*, 3308−19.
(47) Ding, L.; Gao, L. J.; Gu, P. Q.; Guo, S. Y.; Cai, Y. Q.; Zhou, X. T. The role of eIF5A in epidermal growth factor-induced proliferation of corneal epithelial cell association with PI3-k/Akt activation. *Mol. Vision* **2011**, *17*, 16−22.

DOI: 10.1021/acs.jproteome.5b00587
J. Proteome Res. 2015, 14, 3111−3122